Quasi-deuteron model at low renormalization group resolution

A. J. Tropiano , ¹ S. K. Bogner , ^{2,*} R. J. Furnstahl , ¹ and M. A. Hisham , ¹

¹Department of Physics, The Ohio State University, Columbus, Ohio 43210, USA

²Facility for Rare Isotope Beams and Department of Physics and Astronomy, Michigan State University, East Lansing, Michigan 48824, USA



(Received 25 May 2022; accepted 28 July 2022; published 19 August 2022)

Background: The quasi-deuteron model introduced by Levinger is used to explain cross sections for knocking out high-momentum protons in photoabsorption on nuclei. This is within a framework we characterize as exhibiting high renormalization group (RG) resolution. Assuming a one-body reaction operator, the nuclear wave function must include two-body short-range correlations (SRCs) with deuteronlike quantum numbers. In Phys. Rev. C **104**, 034311 (2021), we showed that SRC physics can be naturally accounted for at *low* RG resolution.

Purpose: Here we describe the quasi-deuteron model at low RG resolution and determine the Levinger constant, which is proportional to the ratio of nuclear photoabsorption to that for photodisintegration of a deuteron.

Method: We extract the Levinger constant based on the ratio of momentum distributions at high relative momentum. We compute momentum distributions evolved under similarity RG (SRG) transformations where the SRC physics is shifted into the operator as a universal two-body term. The short-range nature of this operator motivates using local-density approximations with uncorrelated wave functions in evaluating nuclear matrix elements, which greatly simplifies the analysis. The operator must be consistently matched to the RG scale and scheme of the interaction for a reliable extraction. We apply SRG transformations to different nucleon-nucleon (NN) interactions and use the deuteron wave functions and Weinberg eigenvalues to determine approximate matching scales.

Results: We predict the Levinger constant for several NN interactions and a wide range of nuclei comparing to experimental extractions.

Conclusions: The predictions at low RG resolution are in good agreement with experiment when starting with a hard NN interaction and the initial operator. Similar agreement is found using soft NN interactions when the additional two-body operator induced by evolution from hard to soft is included.

DOI: 10.1103/PhysRevC.106.024324

I. INTRODUCTION

Changing the renormalization group (RG) resolution is a powerful technique for analyzing nuclear processes. In this context, the RG resolution is the scale of the largest momentum components in the wave functions of low-energy states. It should not be confused with the experimental resolution that is set by the kinematics of a process and which does not change under RG evolution. In Ref. [1], we showed how evolving to low resolution quantitatively accounts for short-range correlation (SRC) physics phenomenology [2–11] with a cleanly interpreted framework that enables simple yet systematically improvable approximations. More generally, RG evolution enhances scale separation and, hence, factorization of structure and reaction mechanisms, facilitating the extraction of process-independent quantities and correlations between observables. Here we show how the quasi-deuteron model fits into this framework.

The quasi-deuteron model was introduced long ago by Levinger to explain the knock out of high-energy protons in photoabsorption on nuclei at energies of order 100 MeV [12–15]. In particular, the emitted protons were argued to originate from two-body SRCs with deuteronlike quantum numbers (quasi-deuterons) in the nuclear wave function. The quasi-deuterons are induced by the short-range tensor force and repulsive core of phenomenological nucleon-nucleon (NN) interactions. Only proton-neutron (*pn*) pairs are relevant because the dipole term in the photoelectric effect is expected to dominate at the photon energies considered [16]. The picture is that the photon is absorbed by a correlated *pn* pair (the SRC), followed by the emission of the *pn* pair back to back without any further interaction.

The consequence is a proportionality of the photoabsorption cross section of a nucleus with Z protons and N neutrons A = N + Z to that for photodisintegration of the deuteron,

$$\sigma_{A}(E_{\gamma}) = L \frac{NZ}{A} \sigma_{d}(E_{\gamma}), \tag{1}$$

where E_{γ} is the energy of the photon. The Levinger constant L is independent of energy as the cross sections have the same

^{*}bogner@frib.msu.edu

[†]hisham.3@buckeyemail.osu.edu

¹We suppress here a factor that accounts for Pauli blocking in the final state [14,17,18].

energy dependence, dictated by factorization of short-distance physics [1]. In Ref. [13], Levinger approximated the ratio of cross sections as an energy-independent ratio of squared wave functions at small separations,

$$\frac{|\psi_k|^2}{|\psi_d|^2} \approx L \frac{NZ}{A},\tag{2}$$

where ψ_k and ψ_d are the in-medium pn pair and deuteron wave functions, respectively. The in-medium pn pair wave function and the deuteron wave function of Ref. [13] are proportional in the region of small separation r, hence, the ratio yields an r-independent expression in Eq. (2). The factor NZ/A follows from scaling by the number of pn pairs so that L is a dimensionless measure of the density of quasi-deuterons. Equation (2) shows that the cross-section ratio effectively counts the relative probability of quasi-deuterons in a nucleus. See Ref. [19] for a detailed discussion and derivation of the quasi-deuteron model. Assuming the quasi-deuteron model is a good approximation, L is a ratio of measurable quantities, and is, therefore, scale and scheme independent.

A modern treatment of SRCs by Weiss and collaborators relates the Levinger constant to so-called "nuclear contacts" in a model called the generalized contact formalism (GCF) [16,20,21]. In these references, the A/d photoabsorption cross-section ratio is expressed in terms of nuclear contacts, which measure the probability to find two unlike nucleons close to each other. Therefore, the ratio gives the relative probability of finding SRC pairs in the nucleus. The manybody wave-function Ψ is factorized into an asymptotic pair wave-function $\phi_{ij}(\mathbf{r}_{ij})$ and A_{ij} , which is the regular part of Ψ describing the residual A-2 system and depends on the contacts. The $\phi_{ij}(\mathbf{r}_{ij})$ wave function is fixed in the two-body system and, thus, cancels in the ratio of cross sections, leaving dependence on the contacts only.

At high relative momentum, the ratio of momentum distributions is given by contacts as well [20]:

$$\frac{F_{pn}(X)}{n_p(^2H)} \approx \frac{C_{pn}^{s_2=0}(X) + C_{pn}^{s_2=1}(X)}{C_{pn}^{s_2=1}(^2H)},$$
 (3)

where X represents the nucleus and $C_{pn}^{s_2}$ are the pn contacts with total spin s_2 . Using the pn contacts, L is shown to be proportional to the ratio of the pn pair relative momentum distribution F_{pn} and the proton momentum distribution of the deuteron $n_p(^2\mathrm{H})$,

$$\frac{F_{pn}(X)}{n_p(^2\mathrm{H})} \approx L \frac{NZ}{A}. \tag{4}$$

Consistent with the quasi-deuteron model, which assumes only two-body contributions, Weiss *et al.* truncate three-body correlations under the assumption that they contribute much less than the two-body correlations [21].

The RG offers an alternative analysis that is simple and universal. The picture that emerges for the considered photoabsorption kinematics is that the single-nucleon reaction operator that dominates at high RG resolution evolves to include a dominant *two-body* operator at low RG resolution. The quasi-deuteron model is now manifested as this two-body operator that is common to nuclear photoabsorption and

deuteron photodisintegration. Factorization of reaction and structure (rather than factorization of the many-body wave function as in the GCF) makes clear that the Levinger constant only involves long-distance physics that should be well treated by simple approximations and amenable to systematic corrections.

In this paper, we extract the Levinger constant using the ratio of momentum distributions at high relative momentum as in Eq. (4). Our predictions utilize interactions ranging from Argonne v18 (AV18) [22] to soft χ EFT interactions. To account for the scale dependence associated with different interactions, we must include an additional induced two-body operator found by applying inverse-similarity RG (-SRG) transformations of a harder potential. This is analogous to reaction operators inheriting the RG scale and scheme of the underlying Hamiltonian. In an exact low RG resolution calculation, every component in the transition matrix element must be SRG evolved: the initial and final states, and the electromagnetic operator. Each component would change: however, due to the unitarity of SRG transformations, the matrix element would stay the same preserving the cross section. In this picture, the induced two-body operator acting on low-momentum nucleons described by an uncorrelated initial state is responsible for ejected high-momentum nucleons. References [23,24] demonstrate these concepts for deuteron electrodisintegration, although the consequences follow more generally for breakup and knockout reactions.

In Sec. II we provide the necessary formalism for the low-resolution treatment, building on the developments in Ref. [1]. Results are given in Sec. III for several nuclei and compared with experimental extractions. We also examine scale and scheme dependence in extracting *L* under various NN interactions. Section IV has a summary and outlook.

II. FORMALISM AT LOW RG RESOLUTION

SRG transformations when applied to NN potentials decouple momentum scales, through the suppression of off-diagonal momentum-space matrix elements [25–28]. A common decoupling scheme is to drive the potential to band-diagonal form in momentum space as a function of the flow parameter λ , where λ^2 roughly measures the width of the band-diagonal potential with respect to relative momentum squared. Unevolved potentials start at $\lambda = \infty$ and are typically evolved to some finite value of λ by integrating the flow equation,

$$\frac{dV_{\lambda}}{d\lambda} = -\frac{4}{\lambda^5} [\eta_{\lambda}, H_{\lambda}],\tag{5}$$

where H_{λ} is the evolving Hamiltonian and η_{λ} is the anti-Hermitian SRG generator defined as the commutator $\eta_{\lambda} = [G_{\lambda}, H_{\lambda}]$. In practice, the operators in (5) are matrices in (discretized) relative partial-wave momentum space and the flow is solved as coupled differential equations for each matrix element of V_{λ} . Choosing the operator G_{λ} specifies a decoupling scheme. In this paper we set $G_{\lambda} = H_{\lambda}^d$, that is, the diagonal of the evolving Hamiltonian. Other operators can be evolved either by solving an analogous flow equation to (5) or by applying SRG transformations directly. In the latter case, one can construct the transformations from the eigenvectors of the initial and evolved Hamiltonians (see Refs. [29,30] for details on operator evolution).

In this paper we take $\lambda = 1.35 \text{ fm}^{-1}$ as a representative low-resolution RG scale for nuclear ground states that sets the dividing line between low and high momenta. This separation of momentum scales has significant implications when applying consistently evolved operators that probe a high-momentum scale q. Decoupling in the potential leads to suppression of momenta above λ in low-energy states, hence, low resolution. For $q \gg \lambda$, high-momentum operator expectation values are factorized into a product of a universal two-body function encompassing the high-momentum dependence, and a state-dependent matrix element sensitive only to low momenta. This contrasts to factorization in the GCF where the nuclear wave function factorizes into a universal two-body wave function and a contact-dependent term. The details of factorization from the SRG standpoint can be found in Refs. [29,31], and a schematic version is presented in Ref. [1]. For clarity, we will use q to denote the highmomentum scale and k for the low-momentum scale.

At low RG resolution we calculate momentum distributions by using SRG transformations to evolve initial operators (truncating three-body and higher contributions) and evaluate nuclear matrix elements under simple approximations. As in Ref. [1], we will use a local-density approximation (LDA) and average over local Fermi momentum $k_F^{\tau}(R)$ to evaluate nuclear matrix elements. For brevity we will only repeat the key points in this section whereas further details can be found in Ref. [1].

The SRG unitary transformation at flow parameter λ has the following form in second quantization:

$$\widehat{U}_{\lambda} = \widehat{I} + \sum \delta U_{\lambda}^{(2)} a^{\dagger} a^{\dagger} a a$$

$$+ \sum \delta U_{\lambda}^{(3)} a^{\dagger} a^{\dagger} a^{\dagger} a a a + [4\text{-body}] + \cdots, \qquad (6)$$

where we have suppressed the single-particle indices and combinatoric factors. In practice, $\delta U_{\lambda}^{(2)}$ is calculated in relative partial-wave momentum states of the two-body system alone; in the present approximation, $\delta U_{\lambda}^{(3)}$ does not contribute. As mentioned in Sec. I, it is sufficient to extract the Levinger constant from the ratio of momentum distributions at high relative momentum. We apply SRG transformations to the momentum distribution operators and use Wick's theorem in operator form to truncate at the two-body (vacuum) level (i.e., omit $a^{\dagger}a^{\dagger}a^{\dagger}aaa$ and higher-body operators). For example, in evaluating the pair momentum distribution for two nucleons with isospin projections τ and τ' , respectively, we expand and truncate

$$\widehat{n}_{\lambda}^{\tau,\tau'}(\mathbf{q},\mathbf{Q}) = \widehat{U}_{\lambda} \widehat{n}_{\infty}^{\tau,\tau'}(\mathbf{q},\mathbf{Q}) \widehat{U}_{\lambda}^{\dagger}, \tag{7}$$

where the unevolved $(\lambda = \infty)$ pair momentum distribution operator is

$$\widehat{n}_{\infty}^{\tau,\tau'}(\mathbf{q}, \mathbf{Q}) = \frac{1}{2} \sum_{\sigma,\sigma'} a_{\mathbf{Q}/2+\mathbf{q},\sigma\tau}^{\dagger} a_{\mathbf{Q}/2-\mathbf{q},\sigma'\tau'}^{\dagger} a_{\mathbf{Q}/2-\mathbf{q},\sigma'\tau'}$$

$$\times a_{\mathbf{Q}/2+\mathbf{q},\sigma\tau}. \tag{8}$$

Here \mathbf{q} is the relative momentum, and \mathbf{Q} is the center-of-mass momentum.

An SRG-evolved low-energy state, e.g., the ground state of a nucleus, only has low-momentum components $k < \lambda$. If we take the matrix element of the SRG-evolved distribution (7) at high-momentum $q \gg \lambda$ in such a state, this high-momentum tail will be dominated by a term proportional to $\delta U_{\lambda}^{(2)}(\mathbf{k},\mathbf{q})\delta U_{\lambda}^{\dagger\,(2)}(\mathbf{q},\mathbf{k})$ [1]. For $k < \lambda \ll q$, the SRG transformation factorizes $\delta U_{\lambda}^{(2)}(\mathbf{k},\mathbf{q}) \approx F^{\mathrm{lo}}(\mathbf{k})F^{\mathrm{hi}}(\mathbf{q})$, where the labels "hi" and "lo" in the functions $F^{\mathrm{hi}}(\mathbf{q})$ and $F^{\mathrm{lo}}(\mathbf{k})$ refer to the separation of momentum scales above and below λ . Thus, at high momentum, SRG-evolved momentum distributions factorize as discussed previously. For example, the pair momentum distribution operator at high relative momentum, after truncating to two-body terms, is given by

$$\widehat{n}_{\lambda}(\mathbf{q}, \mathbf{Q}) \approx |F^{\text{hi}}(\mathbf{q})|^{2} \sum_{\mathbf{k}, \mathbf{k}'}^{\lambda} F^{\text{lo}}(\mathbf{k}) F^{\text{lo}}(\mathbf{k}')$$

$$\times a_{\mathbf{Q}/2+\mathbf{k}}^{\dagger} a_{\mathbf{Q}/2-\mathbf{k}}^{\dagger} a_{\mathbf{Q}/2-\mathbf{k}'} a_{\mathbf{Q}/2+\mathbf{k}'}, \qquad (9)$$

where we have suppressed the spin and isospin labels.

Extracting the Levinger constant involves taking a ratio of the expectation value of the operator (9) in a specified nucleus A with the same expectation value in the deuteron. The proton distribution operator in the deuteron is given by a similar expression as Eq. (9) and also factorizes for $q \gg \lambda$. We integrate over the center-of-mass momentum Q in evaluating the relative pair momentum distribution, leaving a ratio dependent only on q, and after applying factorization, we obtain

$$\frac{n_{pn}^{A}(q)}{n_{p}^{d}(q)} \propto \frac{\left|F_{pn}^{\text{hi}}(q)\right|^{2}}{\left|F_{d}^{\text{hi}}(q)\right|^{2}} \frac{\int \langle A|F_{pn}^{\text{lo}}(k)F_{pn}^{\text{lo}}(k')|A\rangle}{\int \langle d|F_{d}^{\text{lo}}(k)F_{d}^{\text{lo}}(k')|d\rangle} \tag{10}$$

for $q \gg \lambda$. The soft wave functions restrict the integrals over k and k' to low momenta.

All partial-wave channels contribute in the numerator of Eq. (10) though the ${}^3S_1 - {}^3D_1$ channel dominates (see Table I in Ref. [1]). With the denominator (deuteron) taking contributions solely from the ${}^3S_1 - {}^3D_1$ channel, the two-body high-momentum functions $F_{pn}^{\rm hi}(q)$ and $F_d^{\rm hi}(q)$ roughly cancel, leaving a low-momentum ratio that is approximately scale and scheme independent and independent of $q \gg \lambda$. The ratio is a "mean-field" quantity, meaning it only depends on soft ground-state wave functions. This is effectively the same as a ratio of GCF contacts. We can then extract the Levinger constant from the low-momentum ratio using Eq. (4).

III. RESULTS

In evaluating the soft matrix elements Eq. (10), we use densities from the Gogny functional [32] for the LDA and evolve the operators to $\lambda = 1.35 \text{ fm}^{-1}$ including only *S*-wave contributions [1]. We have made the same calculations with densities from the SLy4 Skyrme functional [33] using the HFBRAD code [34] and found nearly identical trends. The contribution of higher partial waves is not significant (as documented in Table I of Ref. [1]). We limit results to nuclei

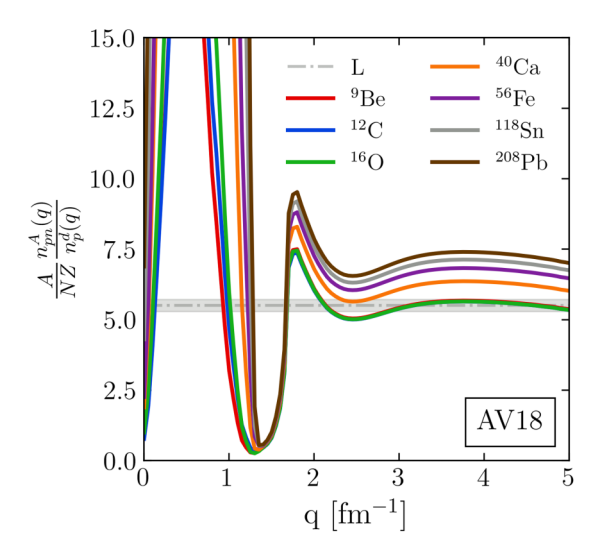


FIG. 1. Ratios of the pn momentum distribution for nucleus A over the deuteron momentum distribution as a function of relative momentum q using the AV18 potential. The gray line and band indicate the average value of the Levinger constant with its error from Ref. [16].

where extractions of L from experimental data are available, although we can easily extend to other nuclei.

In Fig. 1 we show ratios for several nuclei of the pn relative momentum distribution to the proton distribution in the deuteron, scaled by A/NZ. We apply the LDA to both the numerator and the denominator to help cancel systematic errors. At high momentum the ratio plateaus to a constant value, that is, the Levinger constant. The ratio maintains a relatively constant value across high-momentum values despite the momentum distributions individually dropping several orders of magnitude. In the low RG resolution framework, both the numerator and the denominator factorize to a product of a high-momentum two-body function which carries the q dependence, and a low-momentum nuclear matrix element [see Eq. (10)]. The q-dependent functions approximately cancel in the ratio leaving a flat curve where factorization holds $(q \gg$ $\lambda = 1.35 \text{ fm}^{-1}$) as seen in Fig. 1 for all nuclei. The gray band shows the average value of L = 5.5 with its uncertainty across several nuclei [16]. The ratio tends to increase with heavier nuclei. The behavior of the ratio near $q \sim 1.5 \, \mathrm{fm}^{-1}$ depends on the details of the individual momentum distributions near the Fermi surface.

Figure 2 shows our extracted values of L compared to extractions of Refs. [17,35] constrained by cross sections of nuclear photoabsorption experiments [36–39]. In extracting L, we take the average value of the momentum distribution ratios (shown in Fig. 1) over q from 4 to 5 fm⁻¹ as in Ref. [20]. Analysis with other potentials indicates that the factorization holds strongly in the momentum range of 2.5 to 3.4 fm⁻¹ and, consequently, we average over this lower-momentum range as well. Figure 2 shows results from both extraction schemes where the spread from the two schemes is within the black AV18 circles. The low RG resolution calculations are in good agreement with the data and their uncertainties. Calculated values of L monotonically increase with larger mass number

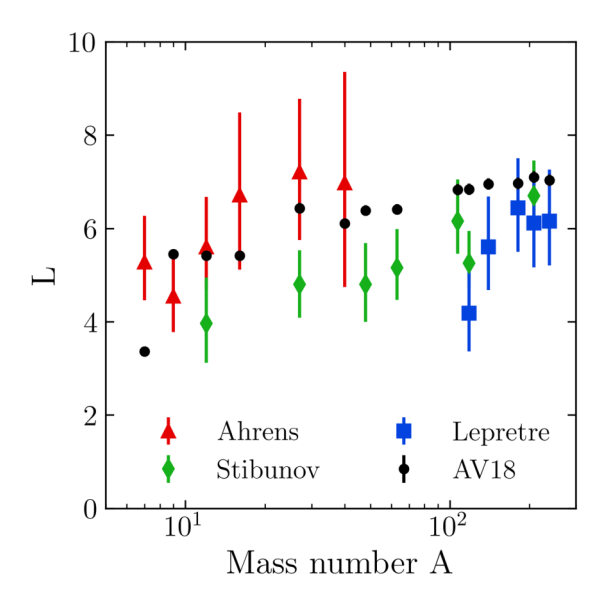


FIG. 2. Average Levinger constant for several nuclei with AV18 comparing to extractions from experiment. The change in predicted L from varying the interval of momentum q over which L is averaged (see the text for details) is smaller than the black AV18 circles.

A similar to the behavior found in calculating the SRC scaling factor a_2 in Ref. [1].

In Fig. 3 we compare Levinger constants between several NN interactions. We show results for AV18 [22], Nijmegen II [40], CD-Bonn [41], SMS N⁴LO [42], and GT+ N²LO [43] averaging over the momentum range of 2.5 to $3.4 \,\mathrm{fm}^{-1}$. We find that the hard potentials (e.g., AV18) produce the highest values of L whereas the soft potentials (e.g., SMS N⁴LO 450 MeV) produce relatively low values. L is extracted from the ratio of inclusive cross sections which, as an observable quantity, is RG invariant; hence, we should not find any significant discrepancies in calculations of L when using

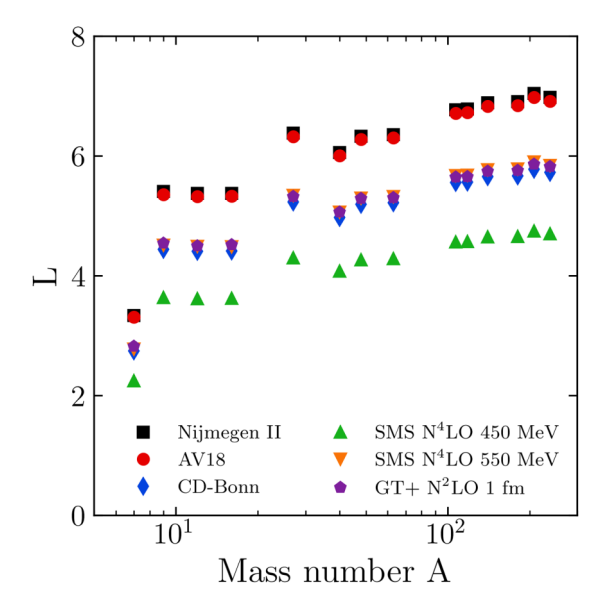


FIG. 3. Average Levinger constant for several nuclei comparing different NN interactions.

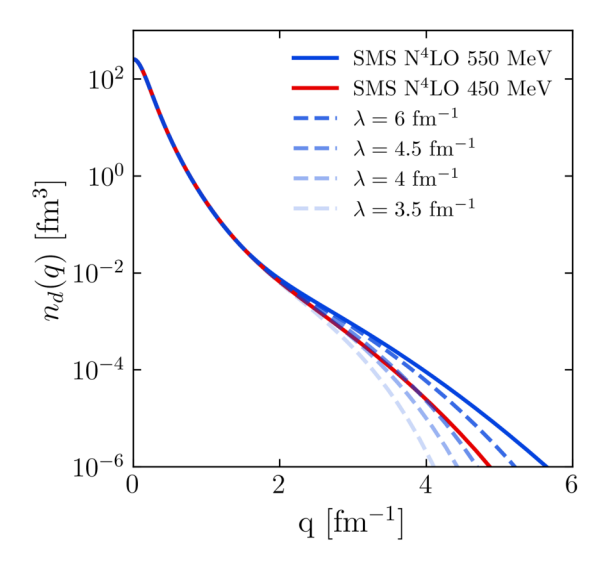


FIG. 4. Deuteron momentum distributions from SMS N⁴LO 550 MeV (blue) and 450 MeV (red) potentials. The dashed lines show the distributions of the 550-MeV potential but SRG evolved to some λ value indicated by the legend.

different NN interactions. However, it is incorrect to assume the same initial operator for interactions at different RG resolution scales.

The momentum distribution is resolution dependent, but we can seek to match the results of *L* using a reference momentum distribution, in this case that of the AV18 interaction. To do so, we must transform the momentum distribution operators of the other potentials for a consistent extraction. For instance, if we take the usual one-body single-nucleon momentum distribution operator when using a hard potential, such as AV18, then we must include an additional two-body contribution in the momentum distribution operator corresponding to the RG resolution scale of the soft potential. In the following, we transform the initial operators of soft potentials to approximately match the results of the hard potentials using the SRG.

We can use SRG transformations to establish an approximate connection between two potentials of different RG resolution scales. To illustrate this, we show the deuteron momentum distributions of the SMS N⁴LO potential at two different regulator cutoffs in Fig. 4. We include snapshots of the deuteron momentum distribution from the SRG-evolved hard potential (550-MeV cutoff). Around $\lambda = 4-4.5 \, \mathrm{fm}^{-1}$ the SRG-evolved deuteron momentum distribution begins to overlap the 450-MeV distribution indicating a rough connection between the two potentials. We find matching scales $\lambda \sim 3.5-5 \, \mathrm{fm}^{-1}$ in comparing other potentials.

We can make similar comparisons in matching interactions by considering Weinberg eigenvalues [44]. These eigenvalues reflect the perturbativeness of a potential and have been analyzed in several RG and EFT studies [25,45–48]. Consider the Born series for the T matrix at energy E given a Hamiltonian $H = H_0 + V$,

$$T(E) = V + V \frac{1}{E - H_0} V + \cdots$$
 (11)

TABLE I. Largest repulsive Weinberg eigenvalues at zero energy for AV18 and SMS N^4LO 550 MeV evolved to several SRG resolution scales λ . The corresponding eigenvalue for the unevolved SMS N^4LO 450 MeV potential is -0.70.

$\lambda \text{ (fm}^{-1})$	AV18	550 MeV
∞	-3.06	-1.22
12	-2.94	-1.27
6	-1.81	-1.10
5.5	-1.61	-1.05
5	-1.40	-0.98
4.5	-1.19	-0.88
4	-0.98	-0.78
3.5	-0.79	-0.66
3	-0.62	-0.54

Solving for the eigenvalues $\eta_{\nu}(E)$ and eigenvectors $|\Gamma_{\nu}\rangle$ of the operator $(E - H_0)^{-1}V$,

$$\frac{1}{E - H_0} V |\Gamma_{\nu}\rangle = \eta_{\nu}(E) |\Gamma_{\nu}\rangle, \tag{12}$$

and applying T(E) on the eigenvectors gives a power series in terms of the Weinberg eigenvalues $\eta_{\nu}(E)$,

$$T(E)|\Gamma_{\nu}\rangle = \left(1 + \eta_{\nu}(E) + \eta_{\nu}^{2}(E) + \cdots\right)V|\Gamma_{\nu}\rangle. \tag{13}$$

Nonperturbative behavior at energy E is signaled by, at least, one eigenvalue $|\eta_{\nu}(E)| > 1$ [44]. For negative energies, purely attractive potentials give positive Weinberg eigenvalues and vice versa for purely repulsive potentials. We refer to positive (negative) eigenvalues with $E \leq 0$ as attractive (repulsive); for E > 0 the eigenvalues become complex.

In comparing interactions, we evolve the harder of the two potentials, compute the Weinberg eigenvalues at zero energy using Eq. (12) in momentum space, and do the same for several SRG-evolved versions of the same potential. Then we compute the corresponding Weinberg eigenvalues of the softer potential and compare to the largest repulsive eigenvalues to determine the matching scale. We document our results for the Weinberg eigenvalues in Table I. This analysis gives roughly the same matching scales as found with comparing deuteron momentum distributions.

In the following, we extract the Levinger constant matching two potentials of different RG resolution scales. We use a scale denoted as λ_m associated with the matching scale from the previous analysis to apply inverse-SRG transformations of the harder potential onto the softer of the two potentials. Figure 5 compares deuteron wave functions of AV18 and SMS N⁴LO 550 MeV, including several inverse-SRG evolved snapshots of the SMS wave function. These are inverse-SRG transformations from the AV18 interaction; hence, the deuteron wave function gains a *stronger* short-range modification as λ_m decreases. At r=0 the inverse-evolved deuteron wave function matches AV18 for λ_m in between 5 and 4.5 fm⁻¹, in agreement with the scale found from analyzing Weinberg eigenvalues.

Taking the inverse-SRG-evolved soft Hamiltonian as the initial Hamiltonian, then evolving that Hamiltonian down to

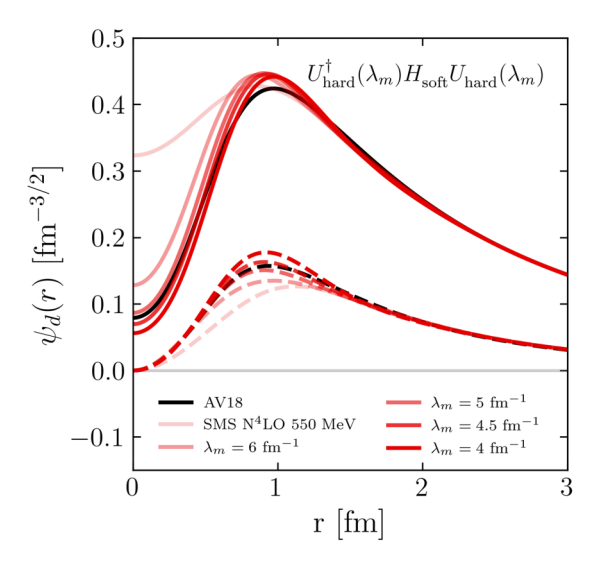


FIG. 5. Deuteron wave functions of AV18 (black) and SMS N^4LO 550 MeV (red) in coordinate space. Additionally, we show deuteron wave functions of SMS N^4LO 550 MeV but inverse SRG transformed with AV18 at several λ_m values. The solid lines correspond to the S states, and the dashed lines correspond to the D states.

 $\lambda = 1.35 \, \mathrm{fm}^{-1}$ in calculating the momentum distribution, is equivalent to applying transformations of the hard potential on the initial operator,

$$\widehat{O}_{\lambda_m} = \widehat{U}_{\lambda_m} \widehat{O} \widehat{U}_{\lambda_m}^{\dagger}. \tag{14}$$

Here \widehat{O} is the initial operator to be used with the hard potential, \widehat{U}_{λ_m} corresponds to transformations of the hard potential $(\lambda_m \approx 4.5 \, \mathrm{fm}^{-1})$, and \widehat{O}_{λ_m} is the initial operator to be used with the soft potential. Consequently, the soft potentials start

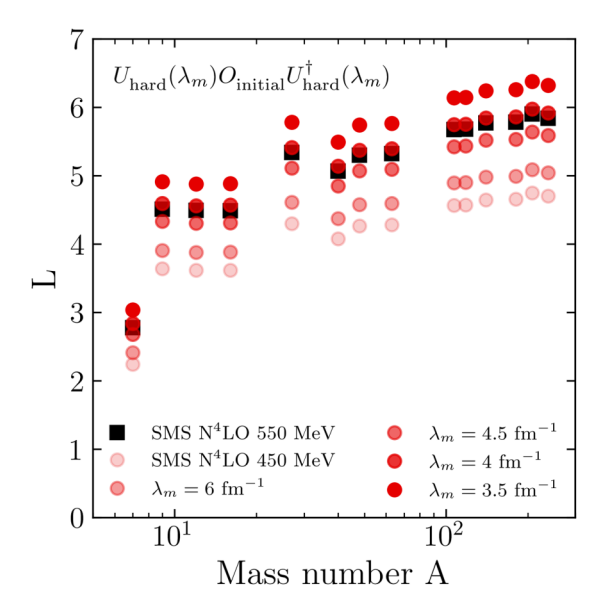


FIG. 6. Average Levinger constant for several nuclei comparing the SMS N^4LO 550 MeV (black) and 450 MeV (red) potentials. Results are also shown for the SMS N^4LO 450-MeV potential with an additional two-body operator due to inverse-SRG transformations from SMS N^4LO 550 MeV at several values of λ_m .

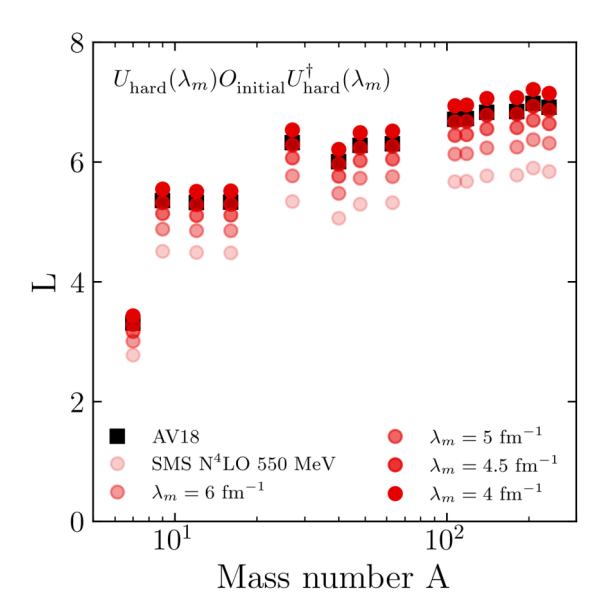


FIG. 7. Same as Fig. 6 but comparing SMS $N^4LO\ 550\,MeV$ to AV18.

with an additional two-body contribution in the operator, whereas hard potentials (such as AV18) start with solely the momentum projection operator (8). Figure 6 compares the two SMS N⁴LO potentials showing results for several λ_m values. We see that the Levinger constants computed from the 450-MeV potential are raised to match the values from the 550-MeV potential around $\lambda_m = 4-4.5 \, \mathrm{fm}^{-1}$, consistent with the deuteron and Weinberg eigenvalue comparisons. These results confirm that an additional two-body operator is necessary in calculating consistent values of L for potentials of a low RG resolution.

In Fig. 7 we make the same comparison as in Fig. 6 but for AV18 and SMS N⁴LO 550 MeV. Here we see that $\lambda_m \approx 4.5 \, \mathrm{fm^{-1}}$ gives the matching scale between the two potentials. Note, this method only serves as an approximate tool in matching interactions, but, in general, there will be additional differences in comparing interactions due to scheme dependence (regulator differences, coordinate- or momentum-space formulations, and so on.)

IV. SUMMARY AND OUTLOOK

We have shown how the Levinger constant can be quantitatively calculated at low RG resolution with simple approximations. This analysis relied on our previous work in using LDA estimates to calculate evolved momentum distributions. The observed scale (and scheme) dependence of the extracted Levinger constants reflects in part insufficient matching of the reaction operator, either to experiment or a more accurate [high-resolution] theoretical description. Additional two-body contributions induced by inverse-SRG transformations on the initial operator restores approximate scale independence.

This strategy demonstrates a more general concept: NN interactions can be "smoothly" connected by RG transformations. The matching can be performed by comparing deuteron

wave functions or Weinberg eigenvalues with consistent results for the matching scale. It may be adequate to incorporate only a contact interaction instead of applying inverse-SRG transformations to match the initial operator to its associated interaction. We leave this point as a follow-up for future work.

The path to more precise determinations is clear. In particular, there are several classes of corrections that need to be examined going forward:

- (1) Incorporating improved many-body physics to test the limits of LDAs and enable uncertainty quantification. The LDA approximation here is implemented as the leading-term in a density-matrix expansion [49]. Including next-to-leading terms is the next step.
- (2) Solving the many-body problem with SRG-evolved operators at different λ values allows for an indirect method in estimating three-body contributions. Residual λ dependence indicates the size of neglected contributions from induced three-body and higher-body terms [50,51]. However, computational restrictions may limit this approach to light nuclei.
- (3) Understanding the impact of long-range correlations and isolating from short-range correlations.
- (4) Better understanding and exploiting the SRG resolution (λ) dependence (e.g., optimal value of λ given our approximations).

To better quantify the impact of common approximations we will directly calculate photoabsorption cross sections, following the low RG resolution calculation of deuteron electrodisintegration [23,24].

A natural follow-up to the present paper is a general examination of level depletion in the RG framework. The results here and in Ref. [1] have explicitly established how processes with particular types of high-energy final states are directly accounted for at low RG resolution by the evolution of basic reaction operators. The converse task is to quantitatively understand at low RG resolution the physics associated at high resolution with depletion of single-particle states [52,53], given that these states are largely occupied in the mean-field picture at low resolution. Here the role of mid-to-long-range correlations are particularly important to understand. This task will involve extending the low RG resolution framework to knockout reactions with electron or nucleon probes. In either case optical potentials play an important role in modeling these processes, and, consequently, we must understand how optical potentials change under RG evolution, which will build on Ref. [54].

ACKNOWLEDGMENTS

We thank A. Garcia for fruitful discussions and feedback, and N. Schunck for sharing a code to calculate Gogny nucleon densities. The work of A.J.T., R.J.F., and M.A.H. was supported by the National Science Foundation under Grant No. PHY–1913069, and the NUCLEI SciDAC Collaboration under U.S. Department of Energy MSU Subcontract No. RC107839-OSU. The work of S.K.B. was supported by the National Science Foundation under Grants No. PHY-1713901 and No. PHY-2013047, and the U.S. Department of Energy, Office of Science, Office of Nuclear Physics under Grant No. de-sc0018083 (NUCLEI SciDAC Collaboration).

^[1] A. J. Tropiano, S. K. Bogner, and R. J. Furnstahl, Phys. Rev. C 104, 034311 (2021).

^[2] O. Hen, G. A. Miller, E. Piasetzky, and L. B. Weinstein, Rev. Mod. Phys. 89, 045002 (2017).

^[3] I. Korover *et al.* (Lab Hall A Collaboration), Phys. Rev. Lett. **113**, 022501 (2014).

^[4] O. Hen et al., Science 346, 614 (2014).

^[5] M. Duer *et al.* (CLAS Collaboration), Nature (London) **560**, 617 (2018).

^[6] M. Duer et al. (CLAS Collaboration), Phys. Rev. Lett. 122, 172502 (2019).

^[7] B. Schmookler *et al.* (CLAS Collaboration), Nature (London) **566**, 354 (2019).

^[8] R. Cruz-Torres *et al.* (Jefferson Lab Hall A Tritium), Phys. Rev. Lett. **124**, 212501 (2020).

^[9] A. Schmidt *et al.* (CLAS Collaboration), Nature (London) **578**, 540 (2020).

^[10] I. Korover *et al.* (CLAS Collaboration), Phys. Lett. B **820**, 136523 (2021).

^[11] J. Arrington, N. Fomin, and A. Schmidt, arXiv:2203.02608 [nucl-ex] (2022).

^[12] J. Heidmann, Phys. Rev. 80, 171 (1950).

^[13] J. S. Levinger, Phys. Rev. 84, 43 (1951).

^[14] J. S. Levinger, Phys. Lett. B 82, 181 (1979).

^[15] J. S. Levinger, Nucl. Phys. A 699, 255 (2002).

^[16] R. Weiss, B. Bazak, and N. Barnea, Phys. Rev. Lett. 114, 012501 (2015).

^[17] M. L. Terranova, D. A. de Lima, and J. D. P. Filho, Europhys. Lett. 9, 523 (1989).

^[18] M. B. Chadwick, P. Oblozinsky, P. E. Hodgson, and G. Reffo, Phys. Rev. C 44, 814 (1991).

^[19] K. Gottfried, Nucl. Phys. 5, 557 (1958).

^[20] R. Weiss, B. Bazak, and N. Barnea, Phys. Rev. C 92, 054311 (2015).

^[21] R. Weiss, B. Bazak, and N. Barnea, Eur. Phys. J. A 52, 92 (2016).

^[22] R. B. Wiringa, V. G. J. Stoks, and R. Schiavilla, Phys. Rev. C 51, 38 (1995).

^[23] S. N. More, S. König, R. J. Furnstahl, and K. Hebeler, Phys. Rev. C **92**, 064002 (2015).

^[24] S. N. More, S. K. Bogner, and R. J. Furnstahl, Phys. Rev. C 96, 054004 (2017).

^[25] S. K. Bogner, R. J. Furnstahl, and R. J. Perry, Phys. Rev. C 75, 061001(R) (2007).

^[26] S. K. Bogner, R. J. Furnstahl, and A. Schwenk, Prog. Part. Nucl. Phys. 65, 94 (2010).

^[27] R. J. Furnstahl and K. Hebeler, Rep. Prog. Phys. 76, 126301 (2013).

- [28] H. Hergert, S. K. Bogner, J. G. Lietz, T. D. Morris, S. Novario, N. M. Parzuchowski, and F. Yuan, Lect. Notes Phys. 936, 477 (2017).
- [29] E. R. Anderson, S. K. Bogner, R. J. Furnstahl, and R. J. Perry, Phys. Rev. C 82, 054001 (2010).
- [30] A. J. Tropiano, S. K. Bogner, and R. J. Furnstahl, Phys. Rev. C 102, 034005 (2020).
- [31] S. K. Bogner and D. Roscher, Phys. Rev. C 86, 064304 (2012).
- [32] J. Decharge and D. Gogny, Phys. Rev. C 21, 1568 (1980).
- [33] E. Chabanat, P. Bonche, P. Haensel, J. Meyer, and R. Schaeffer, Nucl. Phys. A 635, 231 (1998); 643, 441(E) (1998).
- [34] K. Bennaceur and J. Dobaczewski, Comput. Phys. Commun. 168, 96 (2005).
- [35] O. A. P. Tavares and M. L. Terranova, J. Phys. G 18, 521 (1992).
- [36] J. Ahrens et al., Nucl. Phys. A 251, 479 (1975).
- [37] V. N. Stibunov, Sov. J. Nucl. Phys. 40, 1 (1984) [Yad. Fiz. 40, 3 (1984)].
- [38] A. Lepretre, H. Beil, R. Bergere, P. Carlos, J. Fagot, A. Veyssiere, J. Ahrens, P. Axel, and U. Kneissl, Phys. Lett. B 79, 43 (1978).
- [39] A. Leprêtre, H. Beil, R. Bergere, P. Carlos, J. Fagot, A. De Miniac, and A. Veyssiere, Nucl. Phys. A 367, 237 (1981).
- [40] V. G. J. Stoks, R. A. M. Klomp, C. P. F. Terheggen, and J. J. de Swart, Phys. Rev. C 49, 2950 (1994).

- [41] R. Machleidt, Phys. Rev. C 63, 024001 (2001).
- [42] P. Reinert, H. Krebs, and E. Epelbaum, Eur. Phys. J. A 54, 86 (2018).
- [43] A. Gezerlis, I. Tews, E. Epelbaum, M. Freunek, S. Gandolfi, K. Hebeler, A. Nogga, and A. Schwenk, Phys. Rev. C 90, 054323 (2014).
- [44] S. Weinberg, Phys. Rev. 131, 440 (1963).
- [45] S. K. Bogner, R. J. Furnstahl, S. Ramanan, and A. Schwenk, Nucl. Phys. A 784, 79 (2007).
- [46] S. K. Bogner, A. Schwenk, R. J. Furnstahl, and A. Nogga, Nucl. Phys. A 763, 59 (2005).
- [47] S. K. Bogner, R. J. Furnstahl, S. Ramanan, and A. Schwenk, Nucl. Phys. A 773, 203 (2006).
- [48] J. Hoppe, C. Drischler, R. J. Furnstahl, K. Hebeler, and A. Schwenk, Phys. Rev. C 96, 054002 (2017).
- [49] J. W. Negele and D. Vautherin, Phys. Rev. C 5, 1472 (1972).
- [50] E. D. Jurgenson, P. Navrátil, and R. J. Furnstahl, Phys. Rev. Lett. 103, 082501 (2009).
- [51] T. Neff, H. Feldmeier, and W. Horiuchi, Phys. Rev. C 92, 024003 (2015).
- [52] J. A. Tostevin and A. Gade, Phys. Rev. C 90, 057602 (2014).
- [53] T. Aumann et al., Prog. Part. Nucl. Phys. 118, 103847 (2021).
- [54] M. A. Hisham, R. J. Furnstahl, and A. J. Tropiano, arXiv:2206.04809 [nucl-th] (2022).